# Synthesis of poly (3-hexylthiophene-2,5-diyl) in presence of CdS nanoparticles: microscopic and spectroscopic studies

M.E. Nicho[a,b,*], W. Jaimes[a], M.E. Rivas-Aguilar[b], Hailin Hu[c] and M.A. Quevedo-López[b]
[a] *Centro de Investigación en Ingenierías y Ciencias Aplicadas, Universidad Autónoma del Estado de Morelos, Av. Universidad 1001, Col. Chamilpa, 62209, Cuernavaca, Morelos, México.*
[*] *Tel: 0152(777)3297084; fax: 0152(777)3297984.*
*e-mail: menicho@uaem.mx*
[b] *Department of Materials Science & Engineering, University of Texas at Dallas, 800 West Campbell Road, Richardson, Texas 75252, USA.*
[c] *Instituto de Energías Renovables, Universidad Nacional Autónoma de México, Temixco, Morelos 62580, México.*

Received 26 January 2016; accepted 26 July 2016

In this paper, the synthesis of nanocomposites of poly(3-hexylthiophene-2,5-diyl)) (P3HT) and cadmium sulfide (CdS) nanoparticles are reported. CdS nanoparticles were first synthesized using chemical precipitation. Then P3HT was synthesized by direct oxidation of 3-hexylthiophene with $FeCl_3$ as oxidant in presence of CdS nanoparticles. The goal of this work was to investigate the effect of the CdS nanoparticles during the synthesis of P3HT. The resulting films of P3HT/CdS nanocomposites were investigated by Fourier Transform Infrared Spectroscopy (FT-IR), Ultraviolet-Visible Spectroscopy (UV-Vis), X-Ray diffraction, Transmission Electron Microscopy (TEM), Atomic Force Microscopy (AFM) and Scanning Electron Microscopy (SEM). Homogeneous distribution of CdS nanoparticles in P3HT was demonstrated by SEM, AFM and TEM. FTIR analysis showed interaction between CdS and the S atoms of the thiophene rings. This result, together with UV-Vis spectra and XRD patterns suggest a better arrangement of the polymer chains. It is possible that the CdS nanoparticles are coupled with the unpaired electrons of S atoms in the thiophene rings through the positive delocalized charge, resulting in a more ordered P3HT polymer matrix with embedded CdS nanoparticles.

*Keywords:* composite materials; conducting polymers; chemical synthesis; semiconductors; electron microscopy.

PACS: 82.35.Np; 82.35.Cd; 81.07.Pr

## 1. Introduction

Polythiophene derivatives, especially poly(3-alkylthiophenes) (P3AT), are one of the most studied polymers for photoelectronic applications because of their relative stability in air and processability in solution. Poly(3-hexylthiophene) (P3HT) and poly(3-octylthiophene) (P3OT) are of particular interest due to their p-type semiconducting behavior with an electron affinity of $\sim$3 eV and optical band gap of about 2 eV. These polymers are soluble in common organic solvents, contrary to some of the well-known conductive conjugated polymers such as polythiophene, poly(3-methylthiophene), polyaniline, polypyrrole, etc. The photoconductive properties of P3OT films were first described in 1994 [1]. Since then, research on P3OT and P3HT polymers for photovoltaic applications has been extensively investigated. Of particular interest for photovoltaic applications are heterojunctions between P3OT or P3HT with inorganic n-type materials since there is a good match of energetic levels between them for photovoltage generation.

On the other hand, inorganic semiconductor nanoparticles (NPs) have been shown different electronic, photoconductive and luminescent properties compared to ther bulk materials [2,3]. For example, NPs show better charge transfer speeds when chemically bound within an organic polymer matrix. This has enabled their use as acceptors in hybrid solar cell. Hybrid nanocomposites, formed by conducting polymer and semiconductor inorganic nanocrystals (NCs), have been used as volumetric heterojunction structures (BHJ) for solar cell applications and attracted great attention because of the complementary light absorption of each component as well as improved charge carrier collections [4]. A facile method enabling the engineering of the properties for hybrid nanocomposites by simply adjusting the size of nanoparticles and the homogeneous dispersion of the inorganic phase into the organic phase is a key to improve the performance of photovoltaic devices. Among the materials used in hybrid systems poly(3-alkylthiophenes) with cadmium selenide (CdSe) and cadmium sulfide (CdS), has been extensively studied [5-11]. Interest in NPs for applications in inorganic/organic photovoltaic devices increased with the results of CdSe NPs and P3HT system as the active layer in BHJ devices reported by Huynh *et al.* [5]. A common method to prepare such hybrids is to mix inorganic nanoparticles with the conjugated polymer in a common solvent [8]. For example, in Ref. 5, CdSe nanorods were co-dissolved with P3HT in a mixture of pyridine and chloroform and then deposited by spin coating to form a uniform film consisting of CdSe nanorods dispersed in the polymer. It was shown the CdSe nanorods dispersed in P3HT could be oriented to improve charge transport in the resulting photovoltaic device.

The conventional method to prepare hybrid materials involves the use of some surfactant to help the dispersion of NPs in the polymer. This helps to improve the homogeneity

of the NPs distribution in the polymer matrix. However, the surfactant molecules might form an insulating interface between the polymer and the NPs resulting in a degraded charge transport [5,12-14]. Furthermore, mixing pyridine-capped NPs and polymer requires the use of a co-solvent, which can adversely affect NPs solubility and polymer chain orientation. These drawbacks considerably reduce the efficiency of the solar cells. The use of surfactants can be eliminated by either a) developing NPs-conjugated polymer without the use of surfactants and /or ligands, b) directly growing NPs in a polymer solution without surfactants or ligands [15,16], or c) incorporating the NPs during the synthesis of the polymer without surfactants [4]. Demonstration of methods (b) and (c) is limited, especially the last one. Synthesizing the NPs directly in a conducting polymer (b), or synthesizing the conducting polymer in presence of NPs (c) eliminates the need for additional mixing or blending and results in a technique to synthesize nanocomposite materials suitable for optoelectronic applications. Therefore, the development of hybrid materials (Organic/Inorganic) without the use of surfactants and/or ligands has become technically challenging because of its possible benefit for photovoltaic device applications.

Till now only few reports exist for in-situ synthesis of semiconductor nanocrystals in a conducting polymer. For example, in 2004, an in situ synthetic method was used to synthesize PbS nano-crystals/MEH-PPV composites. The authors showed that the polymer chains can sterically stabilize nanocrystal growth in the solution [16,17]. Liao *et al*. [9,18], synthesized CdS single-crystal nanorods directly in the presence of conjugated P3HT, where the polymer was acting as a molecular template to manipulate the CdS nanocrystals and, at the same time, as an efficient charge conductor. A photovoltaic device consisting of CdS nanorods with aspect ratio of ca. 16 and P3HT was assembled and showed a power conversion efficiency of 2.9% under air mass (AM) 1.5. Dayal *et al*. [19], showed the successful synthesis of CdSe nanoparticles in a P3HT-containing solution without the presence of any surfactant, and showed that photo -induced charge separation occurs at the nanoparticle -polymer interface, which is desired for high efficiency photovoltaic solar cells [19]. Sonar *et al*. [20], synthesized CdS and CdSe nanoparticles using a conducting P3HT matrix and determined that P3HT serves as an electrically, thermally and morphologically efficient matrix for the encapsulation of CdS and CdSe nanoparticles, especially for optical and optoelectronic applications. Agrawal *et al*. [21], also synthesized CdS nanocrystals (NCs) in a P3HT matrix by decomposition of a single-molecule precursor. In that work, the final size and the optical band gap of the material depended on the concentration of P3HT and CdS and showed that the growth of CdS NPs in the presence of P3HT is hindered due to its steric effects.

In 2010, Lu *et al.* reported a novel configuration of hybrid solar cells using in-situ polymerization of P3HT on the surface of a $TiO_2$ layer. The short-circuit current density and energy conversion efficiencies of the device with in-situ polymerized P3HT layer were 6X higher compared to that of device without the in-situ polymerized P3HT layer [22]. Subsequently in 2011, Ogurtsov *et al*. reported the synthesis and properties of new hybrid nanocomposites of poly(3-methylthiophene) (P3MT) and CdSe nanoparticles. The synthesis method was based on the chemical oxidative polymerization of 3-methylthiophene in the presence of CdSe nanoparticles [4]. This method allows covering the inorganic nanoparticles with a shell of P3MT. This core-shell structure may have an improved interaction between its components and, as a consequence, could facilitate the charge separation at the donor-acceptor interface. However, P3MT is insoluble in common solvents, whereas P3HT is more suitable for solution based solar cells. In-situ synthesis of P3HT in the presence of nanoparticles promises more and better incorporation of CdS in the polymer composite without the use of surfactants, which would give interesting application in photovoltaic devices [23]. In this work, P3HT/CdS nanocomposites were synthesized by in-situ oxidative polymerization of 3HT in presence of CdS nanoparticles. The results showed an improved interaction between the components of the composites. The effect of CdS nanoparticles in the synthesis of P3HT is studied by using microscopic and spectroscopic techniques, such as Scanning Electronic Microscopy (SEM), Atomic Force Microscopy (AFM), Transmission Electron Microscopy (TEM), Fourier Transform Infrared Spectroscopy (FTIR), UV/Vis spectroscopy and X-ray diffraction (XRD). A reaction mechanism is also proposed.

## 2. Materials and Method

### 2.1. Synthesis of CdS Nanoparticles

In the reported method, a 0.1 M solution of $Na_2S$ (Fermont) and 0.1 M solution of cadmium acetate ($Cd(OOCCH_3)_2 \cdot 2H_2O$, Alfa Aesar, 99.999%) were prepared in methanol. The solution temperature was 25°C (room temperature). The cadmium ion solution was added slowly into the $Na_2S$ solution while stirring constantly. The solution changed from transparent to yellow, indicating that CdS was formed. The reaction time was 30 min. The CdS precipitates were washed by centrifugation at 4400 rpm for 3 min, 3 times with 50 mL of deionized water each time and 2 subsequent times with 50 mL of methanol. The resulting CdS NPs were dried at 50°C for 48 hours [24].

### 2.2. Chemical synthesis of P3HT/CdS nanocomposites

For the synthesis of the P3HT/CdS nanocomposites a weight ratio of 1:2 for 3HT/CdS was used. The P3HT was obtained by direct oxidation of the 3HT monomer (Aldrich, 99%) using Ferric Chloride (Aldrich, $FeCl_3$ 97%) as oxidant at room temperature in an inert atmosphere [25]. In this reaction, 0.0167 mol of distilled 3-hexylthiophene dissolved in anhydrous $CHCl_3$ is slowly added to $FeCl_3$ (0.025 mol) and CdS nanoparticles dispersed in anhydrous $CHCl_3$ (molar ratio 3HT:$FeCl_3$, 1:1.5). The reaction mixture was stirred at

room temperature for 20 h. The product was precipitated in methanol, filtered and carefully washed with methanol, hydrochloric acid (10 vol. %), acetone, $NH_4OH$ (10 vol. %), ethylenediaminetetraacetic acid (EDTA, 1 vol. %) and distilled water. The resulting P3HT/CdS composite was then dried. For comparison, P3HT without CdS NPs was also synthesized following the same procedure.

P3HT/CdS and P3HT films were deposited on Corning glass substrates by spin-coating with a spin frequency of 3000 rpm using a solution with a concentration of 2 mg of polymer by ml solvent (chloroform). Before deposition, the solution was mixed using ultrasound for 20 min. Films were also deposited by drop-casting using the same solution.

### 2.3. Materials Characterization

The surface morphology of P3HT and P3HT/CdS nanocomposites films was studied by SEM (ZEISS SUPRA-40 SCANNING ELECTRON MICROSCOPE). TEM analysis was also carried out. For the TEM analysis, a drop of the CdS/P3HT composite was carefully transferred to a carbon-coated copper grid followed by evaporation of the chloroform solvent. A JEOL 2100F TEM was used for the analysis. AFM measurements of polymer films were carried out with a MFP 3D Bio AFM from Asylum research using the contact mode. FT-IR spectra of P3HT, CdS and P3HT/CdS composites were recorded on a Nicolet 6700 FTIR Spectrometer. Optical characterization of the P3HT and P3HT/CdS films was carried out in a USB4000 Fiber Optic Spectrometer in arrange of 300 to 1000 nm. X-ray diffraction analysis was carried out on a Rigaku MSC Ultima III X-ray diffractometer using a scanning rate of 1 deg/min in $2\theta$ range from 3 to 70°.

## 3. Results and discussion

Figure 1 shows the SEM results of P3HT, CdS and P3HT/CdS composite. CdS nanoparticles synthesized at room temperature showed a homogeneous size and average particle size of about 6.8 nm (Fig. 1a). P3HT polymer was also uniform with no phase separation (Fig. 1b). SEM image of P3HT/CdS nanocomposite (Fig. 1c) showed that the CdS nanoparticles were uniformly distributed in P3HT polymer. Before starting the discussion about the incorporation of CdS nanoparticles in the polymer, we first compare the morphology of P3HT/CdS composites obtained by different sythesis procedures. In the cases of synthesizing the inorganic CdS compooud in the presence of P3HT, micrometer sized agglomerates and CdS nanocrystals were uniformly distributed at the film surface [21]. Furthermore, black spots of 1 $\mu$m size or higher were observed which could be attributed to the aggregation of CdS clusters inside the polymer matrix [20]. In our P3HT/CdS composites the uniform distribution of small CdS particles inside the P3HT matrix could increase the interfacial area between P3HT and CdS and, therefore, benefit the exciton dissociation and charge carrier density of the corresponding solar cells.

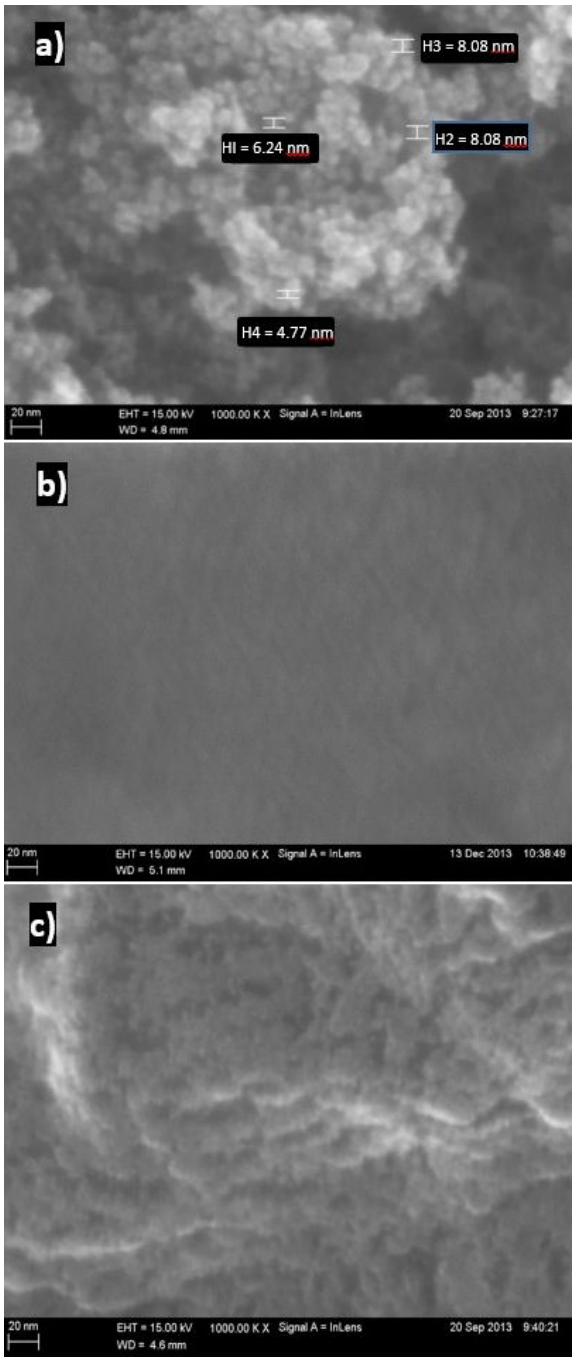


FIGURE 1. SEM images of a) CdS nanoparticles, b) P3HT, and c) P3HT/CdS nanocomposite.

TEM studies were performed on CdS nanoparticles and CdS/P3HT composite (Fig. 2), bright field TEM images (HRTEM), right size. The mean sizes of CdS nanoparticles are in the range of 5-10 nm and their shape is spherical, in agreement with the SEM results. From HR-TEM a plane distance was observed in which the 0.35 nm fringe spacing assigned to the (1 1 1) plane of cubic CdS. The contrast in Fig. 2 indicates the presence of CdS in the P3HT/CdS nanocomposite. The presence of sharper lattice fringes in the high-resolution image (right) shows good crystallinity of the

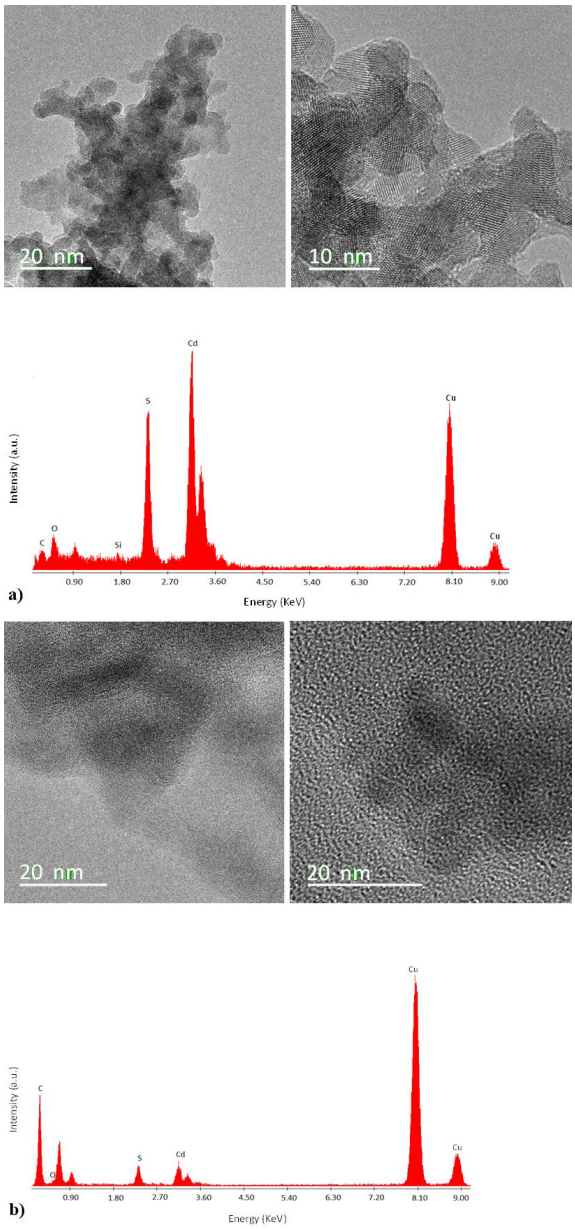


FIGURE 2. TEM images and TEM elemental analysis of a) CdS nanoparticles, b) P3HT/CdS nanocomposite. Right side, bright field TEM images.

P3HT/CdS. Figure 2b shows that CdS is incorporated in the nanocomposite. The CdS nanoparticles showed small clusters into P3HT because no stabilizer or agent were added to the CdS nanoparticles to prevent such agglomeration. The size of CdS nanocrystals into composite was around 10 nm. Similar HRTEM images were obtained by Sonar *et al.* [20] for CdS/P3HT composite synthesized by in-situ synthesis of CdS in presence of P3HT, they also obtained size of CdS nanocrystals from 10-30 nm.

On the other hand, TEM elemental analysis (Energy Dispersion X-ray Spectroscopy, EDS) indicated that there is a loss of CdS during the washing process of the P3HT/CdS composite. According to EDS results, the intensities of the peaks corresponding to S and Cd were almost the same.

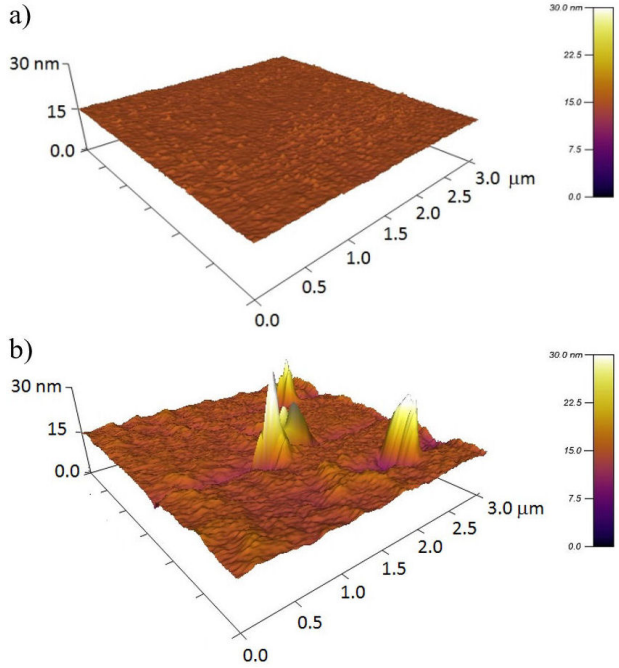


FIGURE 3. AFM images of a) P3HT, RMS: 0.1813 and b) P3HT/CdS nanocomposites, RMS: 1.562.

However, the atomic weight of CdS requires that the peak intensity of Cd should be about 3.5 times than the intensity of S. It means that the extra 2.5 S should come from the 3HT monomer units. Therefore, for every 2.5 3HT monomer units in P3HT there was approximately one CdS nanoparticle. The corresponding weight ratio (2.5:1 for 3HT/CdS) is higher than the initially used in the synthesis (1:2 for 3HT/CdS); the proportion of CdS regarding 3HT fell by one fifth in the composite product. Since CdS could be dissolved in acidic solution, the CdS nanoparticles on the surface of the polymeric membrane probably were dissolved and those CdS nanoparticles inside the polymeric membrane remained after washing by 10 vol.% HCl solution. As a result, the CdS concentration in the product was lower than the initial concentration in the polymerization reaction.

As evidenced from AFM topography for a $3 \times 3$ $\mu$m area (Fig. 3), the morphology of the P3HT/CdS nanocomposites differs from that of P3HT. This is attributed to the presence of the CdS nanoparticles in the nanocomposite. P3HT showed a much smoother topography than the P3HT/CdS nanocomposite; the RMS roughness for P3HT was 0.1813 and for P3HT/CdS was 1.562. The nanocomposite also showed several lumps resulting from agglomerated CdS nanoparticles into the polymer matrix. A similar morphology for P3HT/CdS composites obtained from separated solution of both materials (exhibiting rough "island" structures from large aggregates of QDs) was obtained by Liu *et al.* [26]. However the roughness and lumps size in those composites were higher than in ours, which could affect the interface contact between the active layer and the electrodes [26].

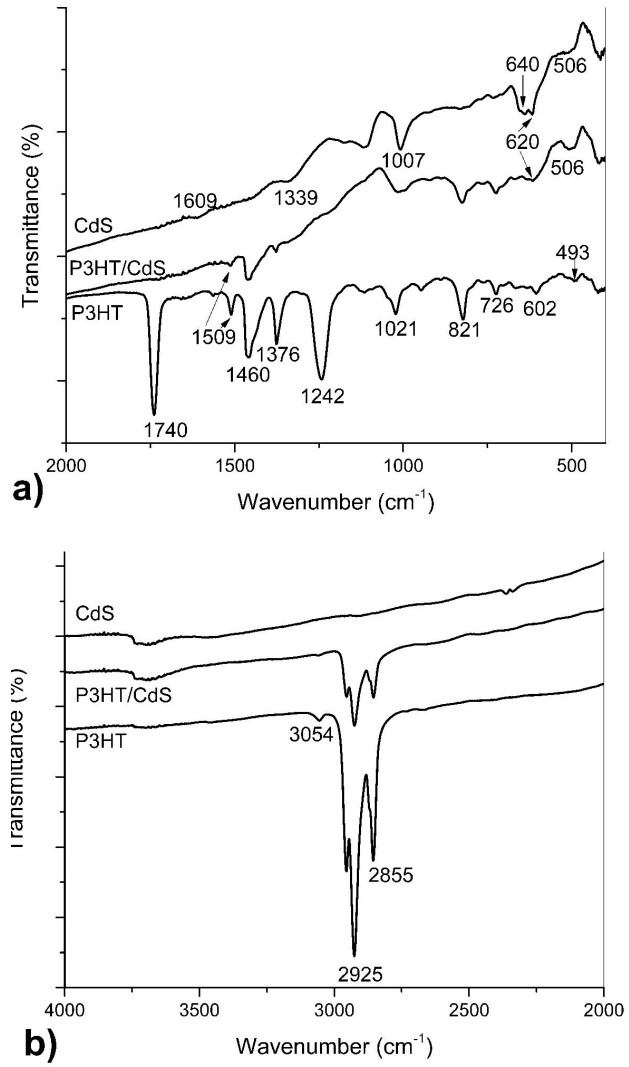


FIGURE 4. FTIR spectra in the frequency range: a) (400-2000 $cm^{-1}$) and b) (2000-4000 $cm^{-1}$) of P3HT, CdS and P3HT/CdS nanocomposite.

To further elucidate the role of CdS during the synthesis of the nanocomposite, Fig. 4 shows FTIR spectra for CdS, P3HT and P3HT/CdS samples in the frequency range of: 400-2000 $cm^{-1}$ (Fig. 4a) and 2000-4000 $cm^{-1}$ (Fig. 4b). The characteristic vibrational bands in the P3HT spectra were located at 3054 $cm^{-1}$ (aromatic C-H stretching vibration of the thiophene ring), at 2955, 2925 and 2855 $cm^{-1}$ (stretching C-H aliphatic, which have been assigned respectively to the asymmetric C-H stretching vibrations of -$CH_3$ moieties, -$CH_2$- moieties, and symmetric C-H stretching vibration in -$CH_2$- moieties) [27]. The two bands at 1460 and 1509 $cm^{-1}$ (aromatic C=C stretching, symmetric and asymmetric) are characteristic of the 2,3,5-trisubstituted thiophene ring. The band at 1376 $cm^{-1}$ corresponds to the methyl bending. The band at 1118 $cm^{-1}$ to the C-S stretching, the band at 821 $cm^{-1}$ to the aromatic C-H out-of plane vibration of a 2,3,5-trisubstituted ring and the band at 726 $cm^{-1}$ to the rocking vibration of hexyl substituent methylene groups-($CH_2$)$_5$-.) [9,28-31]. It is also observed in the FT-IR spectra of P3HT that the bands at 1242 $cm^{-1}$ ($\nu$(C-C) of acetone) and 1740 $cm^{-1}$ ($\nu$(C=O) correspond to acetone. This is likely due to insufficient drying of the samples after washing the products in acetone.

The FTIR spectrum of the CdS nanoparticles is also shown in Fig. 4. The vibration absorption peak of CdS, as reported in literature [32,33] was observed at 410 $cm^{-1}$. The strong absorption band observed at 640 $cm^{-1}$ is probably due to the CdS stretch vibrations [28,34]. The CO symmetrical stretching at 1339 $cm^{-1}$ and CO asymmetrical stretching at 1609 $cm^{-1}$ are likely induced by trace amounts of acetate. The rest of peaks should also come from the impurities presented at the surface of CdS product.

The formation of P3HT-CdS nanocomposites was confirmed by the FTIR spectra as shown in Fig. 4. The intensity of peaks corresponding to C-S bond and aromatic C-H out-of plane stretching decreases and a shift of 5 $cm^{-1}$ for the C-S characteristic band were observed in the P3HT/CdS composite. This indicates a reduction in the C-S bonding energy and suggests intermolecular interaction between S of polythiophene and Cd of the CdS nanoparticle. This interaction should be activated from the original C-S bond by the slight distortion of the electronic cloud of the C-S bond in the thiophene ring. The origin of such intermolecular interaction most likely results from a strong dipole-dipole interaction between the Cd and S atoms, prevailing along the backbone of the P3HT chain [9]. Agrawal *et al*. also reported that the intensity of the peaks corresponding to C-S bond and aromatic C-H out-of plane stretching decreases, which confirmed the chemical interaction between P3HT and CdS in the synthesis of CdS in presence of P3HT [21]. On the other hand, Liao *et al*. [9] observed a slight shift of $\sim$5 wavenumbers to lower energies for the characteristic band of C-S after mixing P3HT and Cd precursor (cadmium acetate). This also suggested an interaction between the $Cd^{2+}$ ions and S atoms. In fact, the CdS nanocrystals are electrically charged ions, thus $Cd^{2+}$ and $S^{2-}$ atoms from the CdS nanocrystals would interact with the thiophene rings in the P3HT molecule. The presence of charges in CdS nanocrystals has been reported elsewhere by R. Smoluchowski [35].

The FTIR spectrum of the CdS/P3HT composite did not show any new bands. However, in the composite, the bands of acetone (1242 $cm^{-1}$ and 1740 $cm^{-1}$) disappeared, probably due to the fact that S atoms in the thiophene ring had already interacted with the CdS when the polymer was washed with acetone. This also confirmed the interaction between CdS and S of the thiophene ring. The absorption band at 1376 $cm^{-1}$ is attributed to methyl bending band. Compared with pure P3HT, the intensity of the absorption band at 1376 $cm^{-1}$ was lower when CdS was added to 3HT in the polymerization reaction. This also confirmed the absence of acetone, due to the loss of the $CH_3$ group of the acetone. Finally, the wide band observed at 1009 $cm^{-1}$ in the composite is due to the 1021 $cm^{-1}$ of P3HT and 1007 $cm^{-1}$ of CdS product, respectively. Also, the band at 620 $cm^{-1}$ is broader

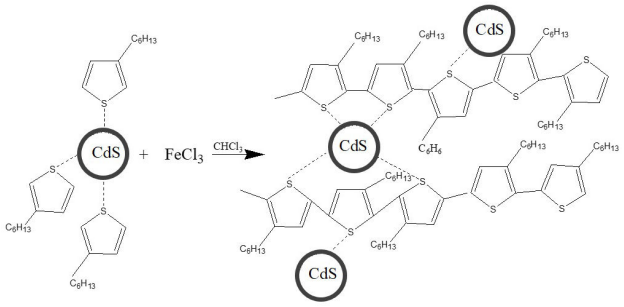


FIGURE 5. Schematic drawing for the proposed synthesis scheme of P3HT/CdS composite. The CdS crystals were assumed to be coupled with the unpaired electrons of S along the P3HT chain network. Proposed mechanism for the growth of the P3HT polymer.

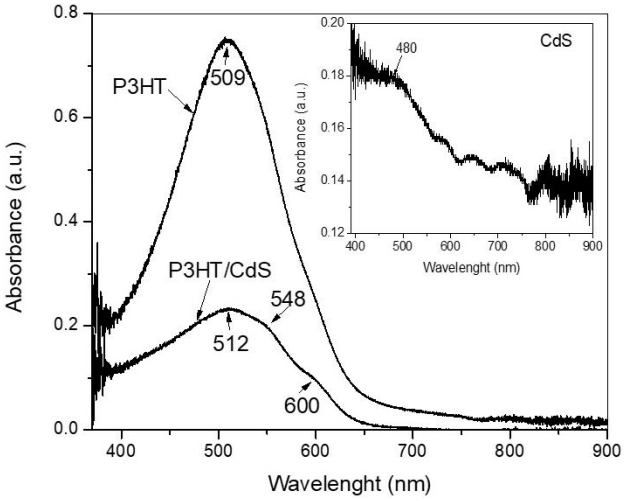


FIGURE 6. UV-Vis absorption spectra of CdS, P3HT and P3HT/CdS nanocomposite films obtained by spin-coating.

due to the superposition of the bands at 602 $cm^{-1}$ (P3HT) and 640 $cm^{-1}$ (CdS). All these findings demonstrated the interaction between CdS and S atom of thiophene ring.

Figure 5 shows the proposed mechanism for the growth of hybrid P3HT/CdS nanocomposites. The delocalized charges of CdS nanoparticles interact with the unpaired electrons in the sulfur of the 3HT monomers resulting in coupling of the two materials. Given the larger size of the CdS nanoparticles ($\sim$7 nm), compared with the P3HT thiophene rings, it is likely that a CdS nanoparticle might interact with more than one thiophene ring. This suggests that a single CdS nanoparticle might interact with more than one polymer chain, resulting in better P3HT stacking, as schematically shown in Fig. 5. As it is known, P3HT polymers obtained by oxidative chemical synthesis are random. The coupling between S in the 3HT monomer and the CdS particles produced some molecular order of P3HT chains, probably due to the lower solidification kinetics in the P3HT/CdS composite film relative to the P3HT film. On the other hand, probably the binding of the contiguous monomeric units 3HT around CdS particles is given in the form of Head-to-Tail (HT) due to the steric effect of the alkyl chains, which causes a larger HT coupling during polymerizing. As such, the CdS nanocrystals may be immobilized in a confined space within the 3HT monomers through a dipole-dipole interaction and pinned during the monomer polymerization. This would result probably in distributed CdS within P3HT, as evidenced by SEM, TEM and AFM (Figs. 1, 2 and 3, respectively).

UV-Vis spectra of regiorandom P3HT and P3HT-CdS nanocomposite of films obtaining by spin-coating on glass substrates are shown in Fig. 6. The inset in Fig. 6 shows the corresponding CdS absorption spectra. The absorption spectrum of regiorandom P3HT thin film shows strong absorption peak at 509 nm. This band is attributed to the excitation of electrons in the $\pi$-conjugated system [36,37]. In UV-Vis absorption spectra of CdS (inset Fig. 6), the maximum at $\sim$480 nm is assigned to the optical transition of the first excitonic state of the CdS nanoparticles [38,39].

The absorption spectrum of the P3HT/CdS thin film obtaining by spin-coating (Fig. 6) shows $\lambda_{\max}$ of $\pi - \pi*$ band at 512 nm with two small shoulders at 548 and 600 nm. The $\pi - \pi*$ band maximum of the P3HT/CdS thin film exhibits a 3 nm red shift relative to the P3HT thin films, indicating a better conjugation in the polymer. Another observation was that the $\pi - \pi*$ band becomes wider in the left side, indicating the quantum size effect of the CdS nanoparticles in the composite. The main absorption range of CdS is almost below 550 nm, therefore, addition of CdS nanoparticles contributes significantly in the absorbance within 300-550 nm range. A similar feature has been observed by Agrawal *et al*. [21] in CdS/P3HT composites by synthesize CdS nanocrystals (NCs) in presence of P3HT. They determined that the addition of CdS NCs contributes significantly in the composites absorbance within 300-550 nm range and reduces the enegy gap. However Sonar *et al*. [20] determined a small blue shift of 3 nm, indicating the band gap in the CdS/P3HT composites increased in comparison with that of pure P3HT. The absorption intensity in the nanocomposite is lower due to scattering caused by the nanoparticles in the P3HT matrix [40]. The UV-Vis spectrum of the composite film shows better-defined shoulders at 548 and 600 nm, relative to P3HT. This feature may be correlated with an increase in molecular order and enhanced hole mobility in the P3HT film [41]. The shoulder at 600 nm is generally attributed to a higher crystallization or ordering of intra-chain interactions in semiconducting polymers. The peak intensity depends on the order degree in the intermolecular chains of the microcrystalline domains [18,42]. Thus the presence of CdS nanoparticles in P3HT increased the delocalization of the $\pi*$ orbital of the in-situ polymerized P3HT, which resulted in the red shift of the absorption spectrum. CdS allowed a better arrangement of the polymer chains, so the peaks in the $\pi - \pi*$ band appear [36].

Liao *et al.* [18] and Sonar *et al.* [20] observed a small blue shift of $\lambda_{\max}$ of $\pi - \pi*$ band in-situ growth of CdS nanocrystals in the P3HT matrix (synthesis route contrary to our work). This indicated that the blue shifts were due to the

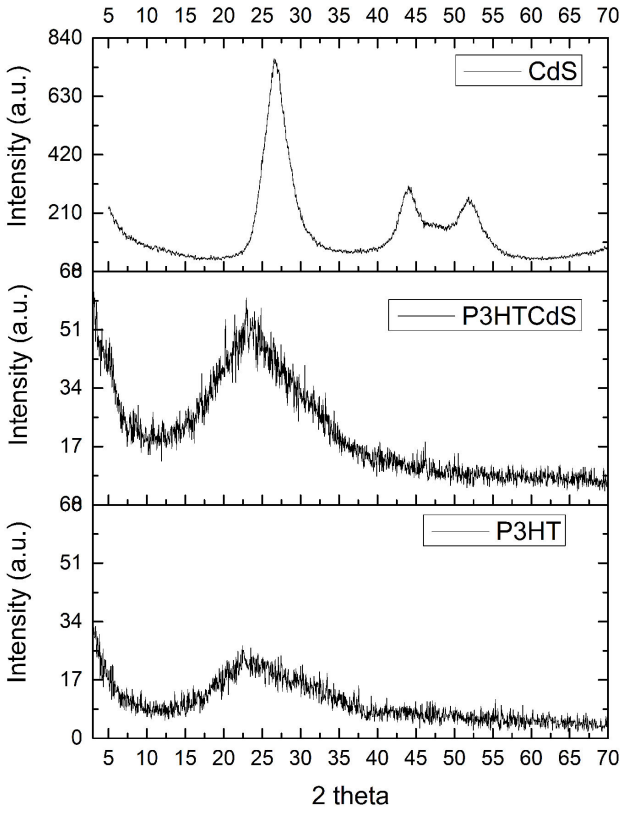


FIGURE 7. XRD patterns for pure P3HT polymer, CdS/P3HT composite and CdS nanoparticles.

in-situ growth of CdS nanocrystals in the P3HT matrix, which induced the consequent destruction of the P3HT chain ordering during solvent evaporation. This blue shift also was observed by Khan *et al*. [40] and Malik *et al*. [43] in preparation of P3HT/CdS composite by mixing solutions of both components (*i.e.* non-in-situ P3HT:CdS blends). Conversely, we determined that in the synthesis of P3HT in presence of CdS nanoparticles, a small red shift of 3 nm ($\lambda_{\max}$ of $\pi - \pi*$ band at 509 nm) was shown, indicating that the band gap in the composites is slightly lower compared with pure P3HT, which was attributed to better ordering of the polymer chains in the composite. The $\lambda_{\max}$ of $\pi - \pi*$ band of our composite (512 nm) was higher than that obtained by Sonar *et al*. (448 nm) in the synthesis in-situ of CdS in presence of P3HT.

Thin films of P3HT/CdS nanocomposites obtained by spin-coating, showed a lower intensities of the $\pi - \pi*$ band than pure P3HT. This suggests that the presence of CdS "diluted" the absorbance of polymer per unit mass or volume, since CdS absorbs poorly at these wavelengths and serves as filler in the polymer. We determined the energy gap for P3HT from the optical density ($\alpha d$) as 1.99 eV and for the composite it was 1.97 eV.

From the UV-Vis absorption it is clear that the P3HT/CdS composite had a higher ordering. This is further supported by the X-ray diffraction (XRD) analysis. Figure 7 shows the XRD pattern of CdS samples synthesized at 25°C for 24 h. The XRD peaks of CdS are very broad indicating very small size, consistent with TEM results. The XRD pattern exhibits prominent, broad peaks at $2\theta$ values of 26.50, 44.00 and 52.1° which corresponds to the 111, 220 and 311 planes of cubic CdS, respectively (JCPDS 10-454) [24,44,45]. The absence of peaks at 28.4 and 53° associated with hexagonal CdS eliminates the possibility of any hexagonal CdS [6].

The semi crystalline nature of P3HT polymer can be seen in the $2\theta$ range of 20°-30° and it was increased in the P3HT/CdS composite. The XRD results for P3HT/CdS shows two small peaks at $2\theta = 5.1$ and 8.8, and one peak at $2\theta = 23.6$. The peak at 8.8 corresponds to the (200) plane of P3HT and the 5.1 peak to the (100) plane from P3HT [46]. XRD analysis shows the appearance of a $\langle 100 \rangle$ peak (alkyl chain spacing, $\pi$-stack direction) for P3HT/CdS composite, confirming a higher degree for P3HT of crystallinity in composite than P3HT. This probably showed evidence of a change in preferential orientation [47]. The appearances of few additional peaks are attributed to the improved crystallinity of the P3HT polymer due to the presence of CdS nanoclusters, thus this result clearly supported the suggestion that the introduction of CdS in the synthesis of P3HT allowed a better arrangement of the polymer chains in P3HT/CdS composites.

From the XRD results it also confirmed the in-situ formation of P3HT with CdS nanoparticles. The CdS nanoparticle signal was not yet visible because, as discussed above, the CdS concentration in the composite was small, and the number of account was low. These results agree with those reported in the synthesis of CdS nanocrystals directly in P3HT matrix with different CdS concentrations [21]. In that case, the crystalline reflections from the CdS nanoparticles became visible in CdS/P3HT composite from a concentration of 1:4 (P3HT:CdS). At concentrations of 1:1 and 1:2 these reflections were not clearly shown, just like what occurred to our composites, and only an increased intensity in the range $2\theta$ of 20°-30° was observed [21]. However, taking into account that the very broad 23.6° peak of P3HT could contain the peak of CdS cubic phase at 26.5°, it is valid to assume that the CdS nanoparticles were within the P3HT polymeric matrix.

Ogurtsov *et al*. found that in the synthesis of P3MT/CdSe nanocomposites by the chemical oxidative polymerization of 3-methylthiophene in the presence of CdSe, the polymerization process is decelerated by CdSe nanoparticles. Specifically, the 3MT polymerization could be realized with a registered rate only at molar ratios of 3MT:$FeCl_3$ = 1:5.34 and 1:13.3, being significantly higher the $FeCl_3$ content than that suitable for the synthesis of individual P3MT (3MT:$FeCl_3$ = 1:2.7). They assumed that the oxidation potential suppression and the existence of the minimal concentration of 3MT could be caused by the side reaction of CdSe oxidation by $FeCl_3$. This side process resulted in the consumption of the oxidant and a partial dissolution of CdSe [4]. In our case, in the synthesis of P3HT/CdS nanocomposites by the chemical oxidative polymerization of 3-hexylthiophene in the presence

of CdS, this phenomenon was not observed, we used the molar ratio 3HT:$FeCl_3$, 1:1.5 and the reaction proceeded.

The P3HT/CdS composite materials are highly promising for use as active film photovoltaic devices.

## 4. Conclusions

Nanocomposites of P3HT/CdS by chemical oxidative polymerization of 3-hexylthiophene in the presence of CdS nanoparticles were successfully synthesized. It was found that the polymerization of P3HT can be carried out was in the presence of CdS. The morphology of P3HT/CdS composite shows an integration of CdS nanoparticles within P3HT; no phase separation of P3HT and CdS nanoparticles was observed. The formation of P3HT/CdS nanocomposites was also confirmed by FTIR analysis, which demonstrated the intermolecular interaction between S atoms of thiophene monomers and CdS. The CdS nanoparticles probably were coupled with the unpaired electrons of S in the thiophene rings through the positive delocalized charge, resulting in the accommodation of CdS nanoparticles along the P3HT chain network. Uniformly distributed CdS nanocrystals within P3HT were evidenced by SEM, AFM and TEM. UV-Vis study showed an increase in molecular order in the P3HT film, which was corroborated by XRD spectra. A small red shift in $\lambda_{\max}$ of $\pi - \pi*$ band of P3HT/CdS nanocomposites was shown, indicating that the band gap in the composites was smaller than that of neat P3HT, which is benefit for solar cell applications.

## Acknowledgments

M.E. Nicho thanks the CONACyT for the fellowship received during her sabbatical stay in the University of Texas at Dallas. The authors acknowledge the financial support received from University of Texas at Dallas, "FONDO SECTORIAL CONACYT-SENER-SUSTENTABILIDAD ENERGÉTICA" through the CEMIE-Sol/27 (project no. 207450) and CONACYT-México CB-2015/255512.

1. G. Yu, K. Pakbaz, A.J. Heeger, *Appl. Phys. Lett.* **64** (1994) 3422.
2. B. Lebeau, P. Innocenzi, *Chem Soc Rev* **40** (2011) 886.
3. H. Dong, H. Zhu, Q. Meng, X. Gong, W. Hu, *Chem Soc Rev* **41** (2012) 1754.
4. N.A. Ogurtsov *et al*., *Molecular Crystals and Liquid Crystals* **536** (2011) 33.
5. W.U. Huynh, J.J. Dittmer, A.P. Alivisatos, *Science* **295** (2002) 2425.
6. R.K. Bhardwaj *et al*., *Materials Letters* **89** (2012) 195.
7. B.R. Saunders, M.L. Turner, *Adv. Colloid Interface Sci.* **138** (2008) 1.
8. B. Sun, N.C. Greenham, *Phys. Chem. Chem. Phys.* **8** (2006) 3557.
9. H.-C. Liao, S.-Y. Chen, D.-M. Liu, *Macromolecules* **42** (2009) 6558.
10. J. De Girolamo *et al*., *A. Pron, Phys. Chem. Chem. Phys.* **10** (2008) 4027.
11. S. Bhattacharya, S. Malik, A.K. Nandi, A. Ghosh, *The Journal of Chemical Physics* **125** (2006) 174717.
12. D. Cui, J. Xu, T. Zhu, G. Paradee, S. Ashok, M. Gerhold, *Appl. Phys. Lett.* **88** (2006) 183111.
13. A.J. Moule, L. Chang, C. Thambidurai, R. Vidu, P. Stroeve, *J Mater Chem* **22** (2012) 2351.
14. S. Zhang, P.W. Cyr, S.A. McDonald, G. Kostantatos, E. H. Sargent, *Appl. Phys. Lett.* **87** (2005) 233101.
15. A.A.R. Watt *et al*., *J. Phys. D: Appl. Phys.* **38** (2005) 2006.
16. A. Watt, E. Thomsen, P. Meredith, H. Rubinsztein-Dunlop, *Chem. Commun.* **20** (2004) 2334.
17. A. Watt, P. Meredith, J.D. Riches, S. Atkinson, H. Rubinsztein-Dunlop, *Curr. Appl. Phys.* **4** (2004) 320.
18. H.-C. Liao, N. Chantarat, S.-Y. Chen, C.-H. Peng, *Journal of the Electrochemical Society* **158** (2011) E67.
19. S. Dayal, N. Kopidakis, D.C. Olson, D.S. Ginley, G. Rumbles, *J. AM. CHEM. SOC.* **131** (2009) 17726.
20. P. Sonar, K.P. Sreenivasan, T. Madddanimath, K. Vijayamohanan, *Materials Research Bulletin* **41** (2006) 198.
21. V. Agrawal, K. Jain, L. Arora, S. Chand, *J Nanopart Res* **15** (2013) 1697.
22. S. Lu, S.-S. Sun, X. Jiang, J. Mao, T. Li, K. Wan, *Journal of Materials Science: Materials in Electronics* **21** (2010) 682.
23. W. Jaimes *et al*., *Materials Science in Semiconductor Processing* **37** (2015) 259-265.
24. C. Martínez-Alonso *et al*., *J Mater Sci: Mater Electron* **26** (2015) 5539.
25. M.E. Nicho, H. Hu, C. López-Mata, J. Escalante, *Sol. Energy Mater. Sol. Cells* **82** (2004) 105.
26. X. Liu *et al*., *Phys. Status Solidi A* **209** (2012) 1583.
27. J.Q. Li, K. Aoki, *J. Electroanal. Chem.* **453** (1998) 107.
28. A. Acharya, R. Mishra, G.S. Roy, *Lat. Am. J. Phys. Educ.* **4** (2010) 603.
29. R.K. Singh *et al*., *Mater. Chem. Phys.* **104** (2007) 390.
30. S. Hotta, S.D.D.V. Rughooputh, A.J. Heeger, F. Wudl, *Macromolecules* **20** (1987) 212.
31. W.Z. Zhang *et al*., *Advanced Materials Research* **704** (2013) 212.
32. R. He *et al*., *Materials Letters* **57** (2003) 1351.
33. Z. Qiao, Y. Xie, J. Xu, Y. Zhu, Y. Qian, *Materials Research Bulletin* **35** (2000) 1355.

34. Z.R. Khan, M. Zulfequar, M.S. Khan, *J Mater Sci* **46** (2011) 5412.
35. R. Smoluchowski, *J. Phys. Colloques* **27** (1966) C3-3.
36. T.A. Chen, X. Wu, R.D. Rieke, *J. Am. Chem. Soc.* **117** (1995) 233.
37. Y.R.D. McCullough, *Adv. Mater.* **10** (1998) 93.
38. R.R. Prabhu, MA. Khadar, *J. Phys.* **65** (2005) 801.
39. L Brus, *J. Phys. Chem.* **90** (1986) 2555.
40. M.T. Khan, R. Bahargav, A. Kaur, S.K. Dhawan, S. Chand, *Thin Solid Films* **519** (2010) 1007.
41. H. Sirringhaus, *Adv. Mat.* **17** (2005) 2411.
42. P.J. Brown *et al*., *Phys. Rev. B* **67** (2003) 064203.
43. S. Malik, S.K. Batabyal, C. Basu, A.K. Nandi, *J. Mater. Sci. Lett.* **22** (2003) 1113.
44. W. Wang, I. Germanenko, M.S. El-Shall, *Chem. Mater.* **14** (2002) 3028.
45. M. Shao, Q. Li, L. Kong, W. Yu, Y. Qian, *J. Phys. Chem. Solids* **64** (2003) 1147.
46. C. Borriello *et al*., *J Appl Polym Sci* **122** (2011) 3624.
47. R.J. Kline, M.D. McGehee, E.N. Kadnikova, J. Liu, J. M.J. Fréchet, *Adv. Mater.* **15** (2003) 1519.